JMEPEG (2012) 21:1777–1784
DOI: 10.1007/s11665-011-0085-z

1059-9495/$19.00

Sintering and Microwave Properties of Zirconium Tin Titanate Doped with Select Oxides

Vera Lucia Arantes

(Submitted January 10, 2011; in revised form October 23, 2011)

Zirconium tin titanate (ZST) is often used as a dielectric resonator for the fabrication of microwave devices. Pure compositions do not sinter easily by solid state sintering; therefore, sintering ZST requires sintering aids capable of creating defects that could improve diffusion processes and/or promote liquid phase sintering. The mechanisms by which the additives influence the microstructure and, consequently, the ZSTs dielectric properties are not very clear. The effects of ZnO, Bi_2O_3, and La_2O_3, on the stoichiometry and dielectric properties of ZST sintered at different temperatures were investigated in this study.

Keywords dielectric resonators, liquid phase sintering, sintering aids, ZST

1. Introduction

The advance of telecommunications, including direct broadcast satellite TV, mobile telephones, and radars during the last 20 years, has demanded the use of ceramic dielectric resonators (DR) with improved properties, such as smaller dimensions and high selectivity. Compared to air cavities, ceramic DRs allow the size of telecommunication devices to be significantly reduced, proportionally to the ceramic's dielectric constant, which favors the miniaturization of microwave devices such as oscillators and filters (Ref 1).

The performance of a dielectric resonator depends on its relative permittivity (ε_r) and quality factor Q ($Q = \tan \delta^{-1}$). It also depends on the thermal stabilities of the relative permittivity ($\tau_{\varepsilon r}$), the resonant frequency (τ_f), and the quality factor, all of which determine the selectivity and attenuation of the dielectric resonator. Thermal stabilities of permittivity, resonant frequency, and quality factor must be as low as possible (Ref 2).

Many systems have been studied as possible candidates for use as DRs: $BaZn_{1/3}Ta_{2/3}O_3$ (Ref 3), barium nonatitanate ($Ba_2Ti_9O_{20}$) (Ref 4, 5), $La(Mg_{1/2}Ti_{1/2})O_3$ (Ref 6), $Ba_8ZnTa_6O_{24}$ (Ref 7), and zirconium tin titanate (ZST) (Ref 8-10). More recently, Reaney and Iddles (Ref 11) have studied complex perovskites and related the order-disorder phase transitions of the perovskites to the performance of the resonators.

Many studies have been performed to maximize the dielectric properties of the systems listed above and to clear up the roles of crystalline structure, phase transformation, and powder characteristics on the performance of microwave ceramics. However, all of the studies employed expensive raw materials or complex powder synthesis processes, factors that need to be minimized for the production of competitive devices.

Compared to other solid solution systems, such as barium nonatitanate (Ref 4, 5) or perovskites (Ref 11), ZST has the best compromise between dielectric properties and ease of preparation. It is the most commonly used material for the production of dielectric resonators.

ZST has an orthorhombic symmetry, with a space group of α-PbO_2, and shows an order-disorder phase transition that depends on the cooling rate during phase transition and the level of Sn-doping (Ref 12, 13). A long-range ordering caused an increase of the dielectric loss, up to 30%, which was not detected when Sn was added intentionally (Ref 13).

It is well known that ZST does not sinter easily by solid diffusion. This has led many researchers to use sintering aids that are capable of creating defects inside the grain or forming a liquid phase. The most popular aids are pure ZnO or ZnO combined with La_2O_3. Other variables that influence the sintered ZST properties are the density, presence and quantity of the second phases, the grain size and type of defects (Ref 14, 15).

Some special processes, such as the sol-gel route (Ref 16) and the hydrothermal synthesis route (Ref 17), have been proposed to obtain pure and fine initial powders, but these processes did not increase the dielectric properties of ZST significantly or lower the sintering temperature.

Comprehending the role of additives on the microstructure and properties of ZST is crucial to maximizing its performance. It has been shown that the sintering aids that create defects are more deleterious to the quality factor than those that do not (Ref 18, 19). Wakino et al. investigated the relationship between the presence of impurities (such as Fe_2O_3 and NiO) and the microstructure of $(Zr_{0.8}Sn_{0.2})TiO_2$ (Ref 18). The incorporation of Fe caused a pronounced decrease in the quality factor, but the simultaneous addition of Fe_2O_3 and NiO did not decrease the quality factor. From the scanning electron microscopy results of the Fe_2O_3-doped samples, exaggerated grain growth and grain distortion were observed. When NiO was added with Fe_2O_3, the phenomena of grain growth and distortion were not detected. In the last case, it was likely that Zn and Ni ions did not diffuse to the grain bulk but formed a second phase in the

Vera Lucia Arantes, Department of Materials Engineering, Engineering School of São Carlos, University of São Paulo, Av. Trabalhador Sancarlense, 400, Pq Arnold Schmidt, São Carlos, SP, Brazil. Contact e-mail: vera@sc.usp.br.

grain boundary and prevented the Fe from diffusing to the interior of the grain. The Fe ions were thought to form a spinel phase with the phase located in the grain boundary.

Iddles et al. studied the influence of ZnO, La_2O_3, and Nb_2O_5 on the properties of $(Zr_{0.875}Sn_{0.25})Ti_{0.875}O_2$ (Ref 19). They attributed the densification of ZST to the formation of a liquid phase zinc titanate, Zn_2TiO_4. During long periods of sintering, ZnO would volatilize and increase the quality factor. At the first stages of sintering, microanalysis showed that La^{3+} ions were located in the grain boundary. As sintering continued, ZnO would volatilize and consequently change the grain boundary composition. The excess TiO_2 and La_2O_3 would then diffuse to the interior of the grain. It was suggested that Ti^{4+} ions occupied their own lattice positions and that La^{3+} ions occupied the available interstitial sites. When the samples doped with only ZnO were compared with those doped with ZnO and Nb_2O_5, the latter had higher Q values. It was believed that Nb^{5+} would compensate the defects in the raw materials that were created by the small amounts of substitutional impurities, such as Fe_2O_3 and Al_2O_3, producing oxygen vacancies in the lattice. A decrease in the amount of oxygen vacancies was responsible for the higher quality factor.

Park et al. also studied the influence of the simultaneous addition of ZnO/Nb_2O_5 as sintering aids. Contrary to Iddles, they concluded that the most important factor that affected the ZST behavior was the sinterability, and this factor would be more important than the creation of defects (Ref 20).

As observed in the work by Kudesia et al. (Ref 15) regarding the effects of La_2O_3 and ZnO on ZST, the grain size of the samples obtained by co-precipitation increased gradually as a function of the sintering aid.

The various works cited above used different sintering aids and distinct sintering conditions with different sintering temperatures, soaking times and heating and cooling rates, but it was difficult to differentiate the influence of distinct sintering aids since the experiments were performed at different sintering conditions. This study focused on the influence of different additives on the dielectric properties of ZST and their effects on the microstructure of ZST. All experiments were done under identical processing parameters, including the pressing and sintering parameters, the sintering temperature and the soaking time.

2. Experimental Procedure

The selected compositions were prepared by mixing the oxides, and the different compositions were designated as follows:

1. ZST0: pure ZST;
2. Z15Zn: ZST + 1.5 wt.% ZnO;
3. Z10Zn: ZST + 1.0 wt.% ZnO;
4. Z05Zn: ZST + 0.5 wt.% ZnO;
5. Z15Bi: ZST + 1.5 wt.% Bi_2O_3;
6. Z15La: ZST + 1.5 wt.% La_2O_3.

The starting materials (ZrO_2, TiO_2, SnO_2, ZnO, La_2O_3, and Bi_2O_3) were all analytical grade with a purity higher than 99.9%. They were ball-milled for 6 h in isopropyl alcohol using stabilized ZrO_2 as a grinding media and PVB as a dispersant. After being dried at 80 °C, the starting materials were calcined at 1120 °C and subsequently ball-milled at room temperature. The process was repeated four times to obtain the maximum reaction rate between the starting oxides (Ref 16).

Cylindrical samples were isostatically pressed at 200 MPa and sintered in air, at temperatures ranging from 1200 to 1450 °C for 6 h. The heating and cooling rates were both maintained at 5 °C/min.

Crystalline phases after calcination and sintering were identified using x-ray diffraction patterns. The samples were irradiated with monochromatized Cu Kα radiation (1.54056 Å) and analyzed between 20° and 70° (2θ).

The apparent density using the Archimedes displacement method with water as the immersing medium and the relative density was calculated by dividing the measured density by the theoretical density.

The microstructures of polished and thermally etched samples were analyzed using scanning electron microscopy (SEM) equipped with quantitative energy dispersive x-ray spectroscopy (EDX).

The grain size was measured using ASTM E112-10 Standard Test Methods for Determining Average Grain Size (Ref 21).

The resonant frequency, relative dielectric constant, and loaded quality factor were measured using cylindrical samples with a thickness and average diameter of 3.50 and 4.85 mm, respectively, the original dimensions of sintered samples. To measure the dielectric constant, a dielectric resonator was placed between two metal plates (Ref 22). When the plates made contact with the dielectric resonator, the field equation could be expressed as an electromagnetic-field equation relating resonant frequency, dielectric constant, and resonator dimensions. The accuracy of the dielectric constant depended on the precision of the measured resonator size and its resonant frequency.

3. Results and Discussion

The starting raw materials were calcined at 1120 °C and ball-milled to induce the reaction between the initial powders and form ZST with a stoichiometry of $Zr_{0.8}Sn_{0.2}TiO_4$. The process was repeated four times. The results of x-ray diffraction are presented in Fig. 1. Both tin and zirconium oxides were completely consumed, but a small amount of TiO_2 remained unreacted despite additional calcination.

3.1 Characterization of ZnO-Doped Samples

In Fig. 2(a), the effect of sintering temperature on the apparent density of the powder is shown for different amounts of ZnO additive. Composition Z10Zn behaved differently when compared to the other three compositions. After an abrupt density increase from samples sintered at 1200 °C to the ones sintered at 1250 °C, the relative density of the sample stabilized between 95 and 98% of the theoretical density. The increase in relative density in such a narrow temperature range is typical of liquid phase sintering. For Z10Zn, the liquid phase formed between 1200 and 1250 °C, which was a higher temperature range compared to the other compositions that incorporated sintering aids. A similar behavior was observed for samples doped with trivalent oxides (Fig 1b). The relative density of the sample with only 0.5 wt.% ZnO had a maximum of 95%

theoretical density. The relative densities of the non-doped samples had a maximum of 95% theoretical density.

The x-ray diffraction analysis of Z15Zn detected the presence of ZST as a major phase. In addition, TiO_2 and Zn_2TiO_4 were in different quantities, as seen in Fig. 3(a). It is worth noting that a small quantity of TiO_2 was detected even after the initial powders were calcined for four times. Zinc titanate (ZT) was observed at 1300 °C in sample Z15Zn. After the sample was sintered at 1450 °C, it only contained the ZST and TiO_2 phases and not the ZT phase. Even though Zn_2TiO_4 was detected only for samples sintered at temperatures above 1250 °C, the densification behavior suggested the phase formed at a lower temperature. The Zn_2TiO_4 phase became a liquid at a temperature lower than that predicted by the phase diagram with the presence of Sn and/or Zr. No ZT phase was detected in the Z10Zn sample (Fig. 3b).

Figure 4 compares the SEM micrographs of Z15Zn sintered at increasing temperatures; the morphological evolution of the second phase, labeled as 1 in the micrograph could also be observed in the figure. Figure 5 presents the quantitative EDX analysis of the grain and the second phase of Z15Zn. Z15Zn contained a Ti-rich second phase that was likely due to the decomposition of Zn_2TiO_4, which was detected by x-ray diffraction. The presence of Zr and Sn in this phase was the result of partial dissolution of ZST grains into the initial liquid phase. The same was observed for Z10Zn, although the amount of the second phase, which had a high percentage of Ti, was lower (Fig. 6). This was attributed to the lower level of ZnO that was added to the ZST in this sample. Furthermore, the amount of free-TiO_2 was derived from the dissolution of the second phase into ZST and TiO_2. The wetting characteristics were clearly influenced by the stoichiometry of the second phase (shown as light grains in Fig. 6), since that, as for Z10Zn, the morphology of the second phase varied with the sintering temperature which, in turn, was responsible for the variation of liquid phase stoichiometry.

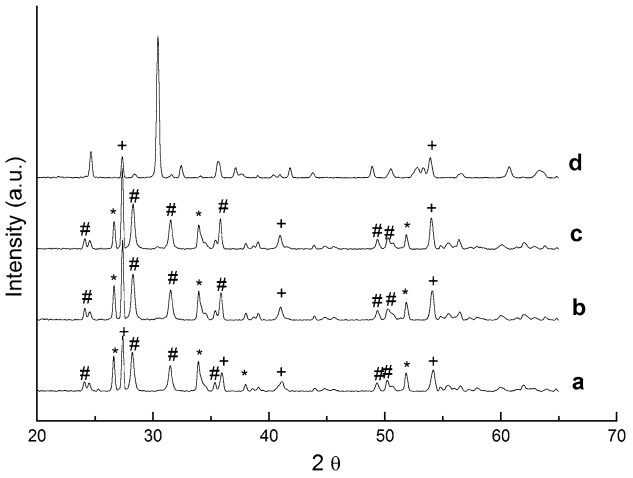

Fig. 1 Evolution of crystalline phases in pure ZST as a function of the sintering temperature. The sample was calcined: (a) once; (b) twice; (c) 3 times; and (d) 4 times

3.2 Characterization of Bi_2O_3 and La_2O_3-Doped Samples

The x-ray diffraction patterns of Bi_2O_3- and La_2O_3-doped ZST samples showed the presence of TiO_2 at a very small amount compared to the ZnO-doped samples. Figure 2(b) shows the apparent density of ZST as a function of sintering temperature for the different compositions. As seen in the figure, the addition of Bi_2O_3 promoted the densification of ZST. However, the densification of ZST was not satisfactory, with only 0.5% of Bi_2O_3. The x-ray diffraction patterns of Bi- and La-doped samples are shown in Fig. 7.

In Fig. 8, one can observe a small difference between the small and large grains in the microstructure of the Z15Bi sample. In SEM images, the lighter grains were deficient in Ti relative to the nominal stoichiometry ($Zr_{0.8}Sn_{0.2}TiO_2$). When the quantitative microanalysis results of the samples sintered at different temperatures were compared, the stoichiometry of the grains showed a marked change after the samples were sintered at 1400 °C (as seen in Fig. 8). This explains the presence of the light grains in the microstructure.

The densification curve and microstructural evolution showed that the use of Bi_2O_3 promoted the formation of a liquid phase that was distinct from the one formed in the ZnO-doped samples. The second phase brought about by the addition of Bi was not capable of promoting dissolution of ZST grains.

Figure 8(c) and (d) show the micrographs and the quantitative EDX data for selected grains of the Z15La sample. The light grains contained a higher percentage of La

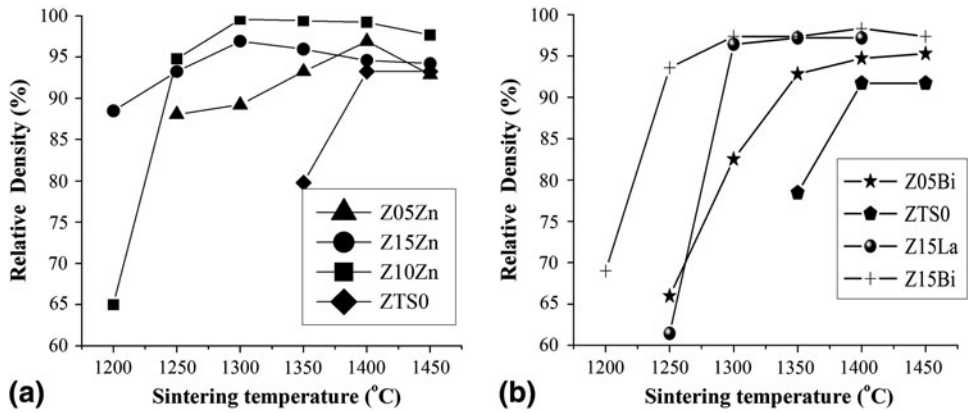

Fig. 2 (a) Evolution of apparent densities as a function of temperature for undoped (pure) and ZnO-doped samples. (b) Apparent density vs. sintering temperature of Z15Bi compared to Z05Bi and ZST0

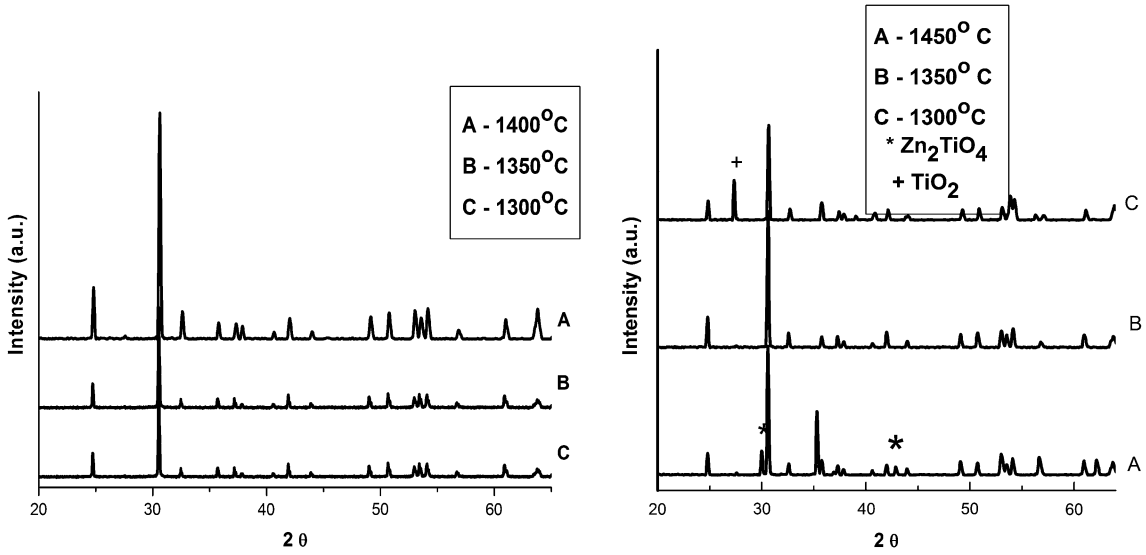

Fig. 3 Evolution of crystalline phases in (a) Z15Zn and (b) Z10Zn as a function of the sintering temperature. The non-indexed peaks refer to ZST

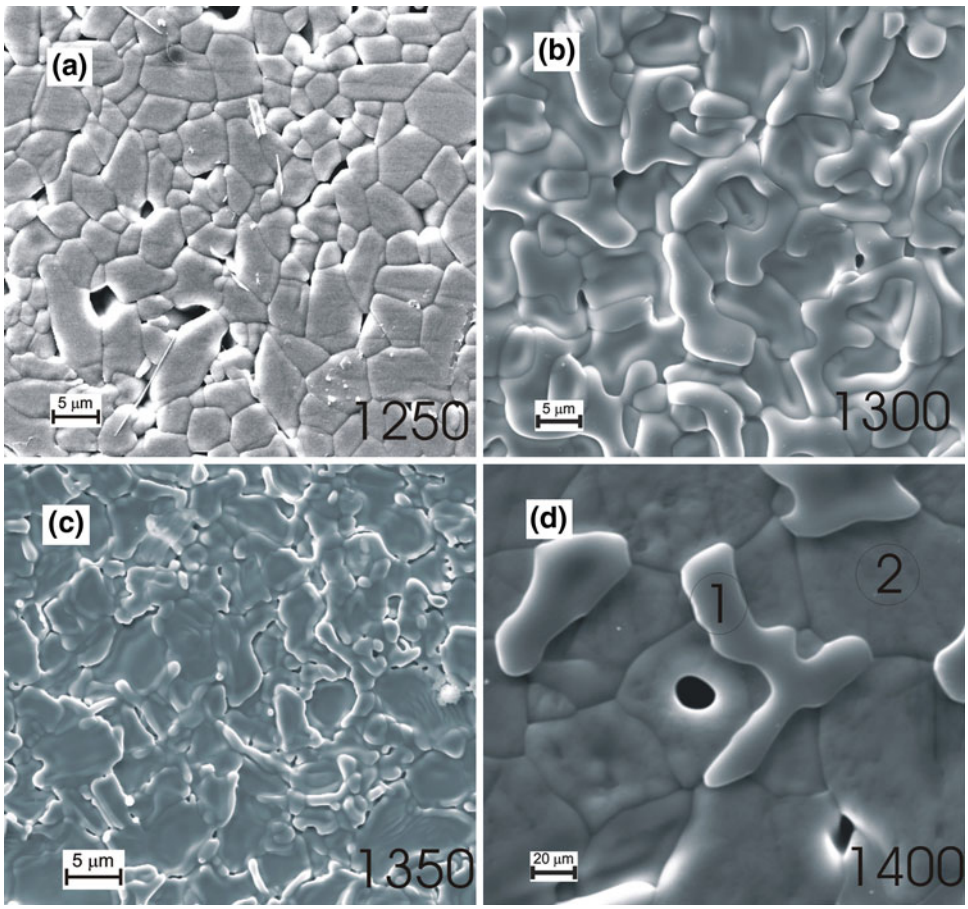

Fig. 4 SEM images of Z15Zn sintered at (a) 1250 °C, (b) 1300 °C, (c) 1350 °C, and (d) 1400 °C for a soaking time of 6 h

(Fig. 8d), which indicated that La was incorporated into the grain. In Fig. 8(c), some small light grains were observed. The EDX data revealed this second phase to be a lanthanum- and titanium-rich phase, which confirmed that La would act interstitially in a ZST unit cell as suggested by other literature data.

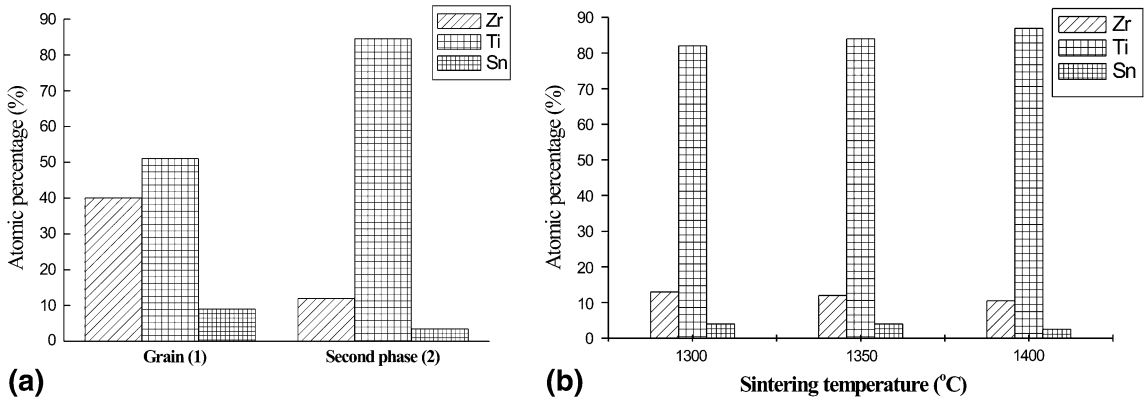

Fig. 5 Quantitative EDX analysis of Z15Zn: (a) as a function of the microstructural position of samples sintered at 1400 °C for 6 h; (b) grain stoichiometry as a function of sintering temperature. The numbers 1 and 2 refer to the numbers in Fig. 4

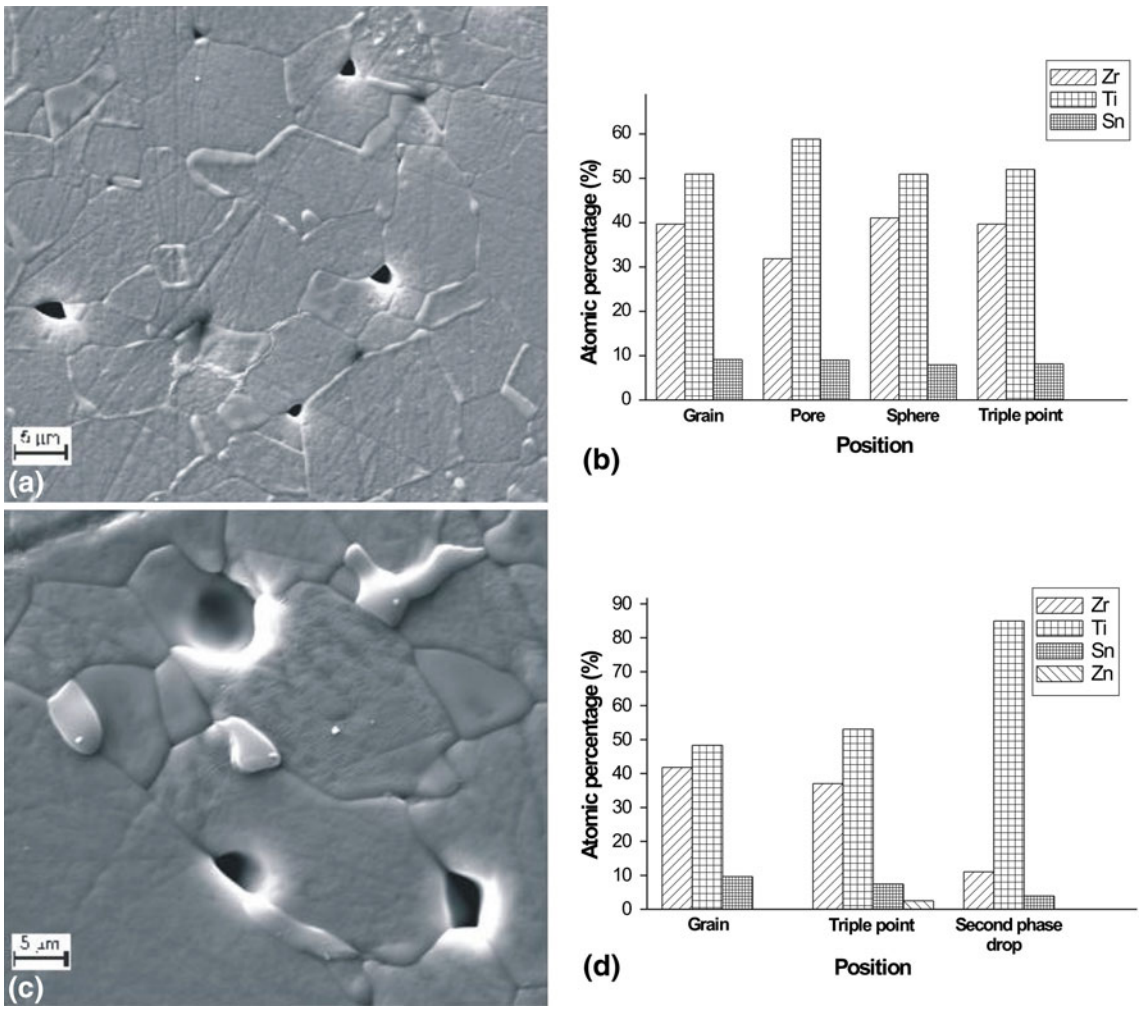

Fig. 6 (a) SEM image of Z10Zn sintered at 1300 °C; (b) quantitative EDX analysis for the sample sintered at 1300 °C; (c) SEM image of Z10Zn sintered at 1400 °C; (d) quantitative EDX analysis for sample sintered at 1400 °C

Adding 1.5% of La_2O_3 gave rise to a monophased dense ZST at 1300 °C, and free-TiO_2 was not detected in samples sintered at temperatures as low as 1200 °C. The densification curve was typical of liquid phase sintering because all densification occurred in a narrow temperature range. In spite of the initial stoichiometric formulation, the final undoped ZST powder showed crystalline ZST and TiO_2 phases, which did not participate of the reaction to form the desired ZTS stoichiometry.

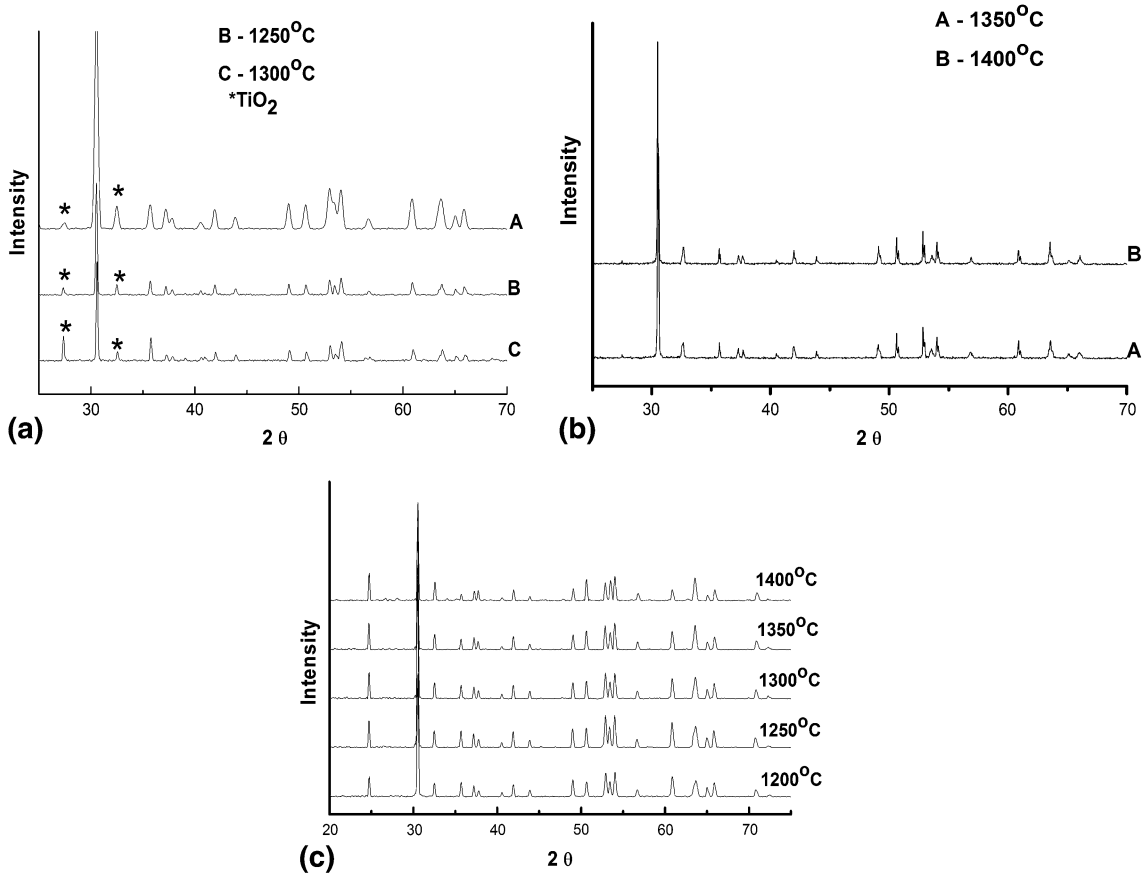

Fig. 7 Evolution of crystalline phases as a function of sintering temperature: (a) Z15Bi sintered at 1200, 1250, and 1300 °C; (b) Z15Bi sintered at 1350 and 1400 °C; (c) Z15La sintered at increasing temperatures; the non-indexed peaks refer to ZST

The EDX results showed that the composition of the liquid phase changed with the sintering temperature and determined the Ti concentration of the ZST grain. The use of Bi_2O_3 promoted densification at the lowest sintering temperature among all samples. The La-doped samples showed a different behavior, compared to the ones doped with others oxides used as sintering aids, because La was incorporated by the grain.

3.3 Dielectric Properties

Table 1 shows the data of dielectric properties, average grain size, and [Ti]/[Zr + Sn] ratios for all studied samples and those for a commercial dielectric resonator. The dielectric constants of the samples were rather similar to the constant of the commercial resonator, but the values of the loaded quality factor, the resonant frequency and the values of $(Q \times f_r)$ varied significantly.

Many researchers have pointed out that the quality factor would increase proportionally with the grain size because a larger grain has a smaller grain boundary area and fewer defects. Consequently, the loss factor would decrease. In this study, the data revealed that a direct relationship did not exist between the grain size and the quality factor, as shown in Fig. 9. Other variables would need to be considered to define the quality factor, such as [Ti]/[Zr + Sn] ratio inside the grain .

Even though sample Z15Zn and sample Z10Zn were both sintered at the same temperature and had similar grain sizes, they had different loaded quality factors due to the different amounts of sintering aid. However, the quality factor of Z15Zn and Z10Zn samples were lower than that of Z05Zn samples. A maximum grain size exists for a unique composition sintered at different temperatures. As observed in the microstructure (Fig. 4), the ZnO that originated from the liquid phase during the sintering of ZST was located in the grain boundary. Depending on the amount of ZnO, the grain stoichiometry could be altered. The stoichiometry changed according to the amount of ZnO and the sintering temperature, even though the second phase had the same elements as the matrix. The parameter responsible for determining the quality factor was the grain stoichiometry, which in turn was dictated by the composition of the liquid phase, as shown in Fig. 10.

For Bi-doped samples, the dielectric constant and the resonant frequency did not vary systematically with the Bi_2O_3 amount and the sintering temperature (Table 1). On the other hand, $Q \times f_r$ decreased with the sintering temperature as a result of the increasing unit cell volume. In this case, the reduction of the loaded quality factor was associated with the perturbation of the crystalline order due to the presence of Bi inside the grains. These defects promoted phonon scattering and consequently increased the dielectric loss. The observed reduction in the unit cell volume (Table 1) was caused by oxygen vacancies that were created to maintain charge neutrality.

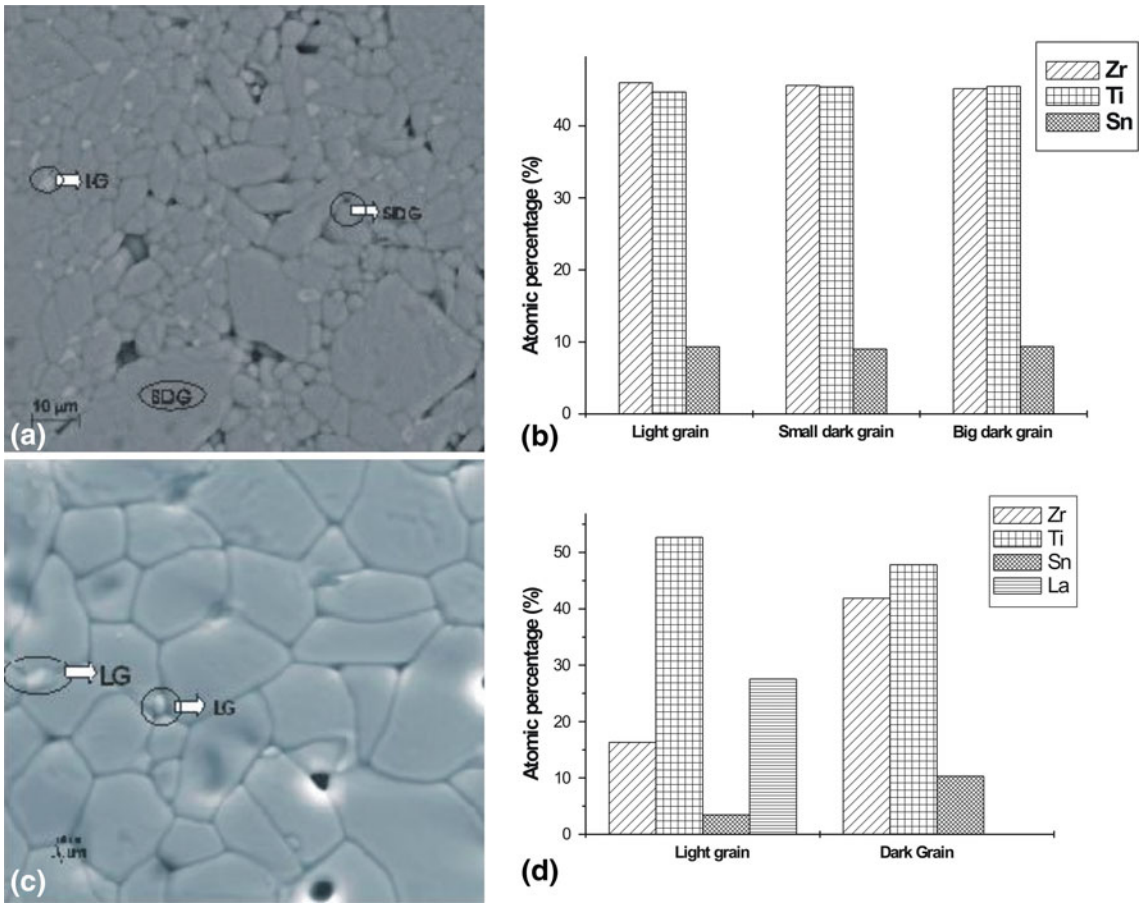

Fig. 8 (a) SEM images of Z05Bi sintered at 1400 °C for 6 h; (b) EDX results of different regions of Z15Bi; (c) SEM images of Z15La sintered at 1400 °C for 6 h; (d) EDX of different regions of Z15La

Table 1 The dielectric properties, average grain size, and [Ti]/[Zr + Sn] ratios of all samples at a high frequency and sintered at various temperatures

Composition	Sintering temperature, °C	Dielectric constant, ε_r	$Q_l \times f_r$	Average grain size, μm	[Ti]/[Zr + Sn] of the grain
Z15Zn	1250	37.6 ± 0.7	12170 ± 48.7	4.7 ± 0.3	…
	1300	38 ± 1.9	12430 ± 62.2	6.6 ± 0.1	1.04
	1400	38 ± 0.3	13180 ± 40.6	13 ± 0.0	1.10
Z10Zn	1250	38.1 ± 0.5	13530 ± 81.2	5.9 ± 0.4	…
	1400	37.3 ± 0.4	15150 ± 75.8	12 ± 0.1	0.94
Z05Zn	1300	38.7 ± 1.2	11220 ± 78.5	8.1 ± 0.1	0.90
ZST0	1450	35.5 ± 0.5	11340 ± 79.4	9 ± 0.7	…
Z15Bi	1250	38.8 ± 0.5	14090 ± 42.3	4.3 ± 0.8	0.87
	1300	39.5 ± 0.3	13150 ± 95.2	4.5 ± 0.4	0.87
	1350	38.9 ± 0.2	11800 ± 59.0	4.7 ± 0.5	0.89
Z15La	1400	39.5 ± 0.2	12940 ± 25.9	7.1 ± 0.1	0.92

4. Conclusion

The influence of different sintering aids on the microstructure and dielectric properties of ZST at microwave frequencies was studied in this work. Both the quantity and the type of additive had a crucial role in the formation of a liquid phase, the presence of secondary phases and the grain stoichiometry. The [Ti]/[Zr + Sn] ratio inside the ZST grain was the most important factor that determined the dielectric properties of ZST at high frequencies.

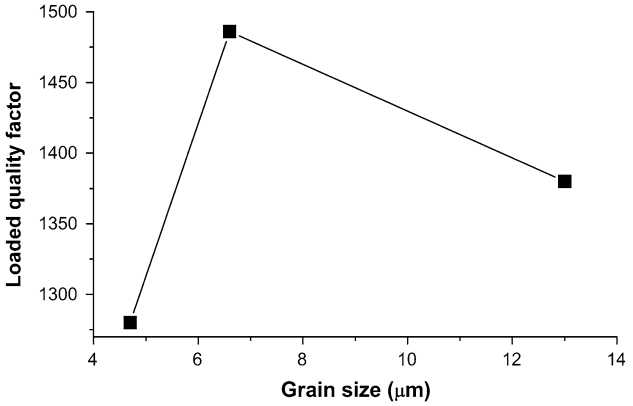

Fig. 9 Quality factor as a function of grain size for Z15Zn

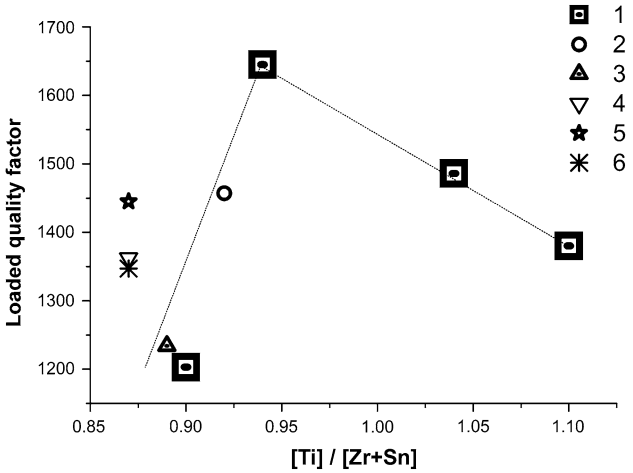

Fig. 10 Loaded quality factor vs. [Ti]/[Zr + Sn] inside the grain for: 1, ZnO; 2, La_2O_3 sintered at 1300 °C; 3, 1.5 wt.% Bi_2O_3 sintered at 1350 °C; 4, 0.5 wt.% Bi_2O_3 sintered at 1300 °C; 5, 1.5 wt.% Bi_2O_3 sintered at 1250 °C; 6, 1.5 wt.% Bi_2O_3 sintered at 1300 °C

Acknowledgments

The authors are thankful for the financial support of Coordination for Improvement of Post-Graduation—CAPES and São Paulo Research Foundation—FAPESP.

References

1. A.J. Moulson and J.M. Herbert, *Electroceramics*, 2nd ed., John Wiley & Sons, West Sussex, 2003
2. W. Wersing, *Electronic Ceramics*, B.C.H. Steele, Ed., Elsevier A. S., London, 1991, p 93–99
3. S. Kawashima, M. Nishida, I. Ueda, and H. Ouchi, $Ba(Zn,Ta)O_3$ Ceramic with Low Dielectric Loss, *J. Am. Ceram. Soc.*, 1983, **66**(6), p 421–423
4. I. Negas, G. Yeager, J. Bell, N. Coats, and I. Minis, $BaTi_4O_9$/$Ba_2Ti_9O_{2O}$-Based Ceramics Resurrected for Modern Microwave Applications, *Am. Ceram. Soc. Bull.*, 1993, **72**(1), p 80–89
5. S. Kumara, V.S. Raj, and T.R.N. Kutty, Preparation of $BaTi_4O_9$ and $Ba_2Ti_9O_{20}$ Ceramics by the Wet Chemical Gel-Carbonate Method and Their Dielectric Properties, *Mater. Sci. Eng. B*, 2007, **142**, p 78–85
6. M.P. Seabra, V.M. Ferreira, H. Zheng, and I. Reaney, Structure Property Relations in $La(Mg_{1/2}Ti_{1/2})O_3$-Based Solid Solutions, *J. Appl. Phys.*, 2005, **97**(3), p 033525-033525-10
7. S.M. Moussa, J.B. Claridge, M.J. Rosseinsky, S. Clarke, R.M. Ibberson, T. Price, D.M. Iddles, and D.C. Sinclair, $Ba_8ZnTa_6O_{24}$: A High-Q Microwave Dielectric from a Potentially Diverse Homologous Series, *Appl. Phys. Lett.*, 2003, **82**(25), p 4537–4539
8. X. Lu, Y. Lee, S. Yang, Y. Hao, R. Ubic, J.R.G. Evans, and C.G. Parini, Fabrication of Millimeter-Wave Electromagnetic Bandgap Crystals Using Microwave Dielectric Powders, *J. Am. Ceram. Soc.*, 2009, **92**(2), p 371–378
9. V.L. Arantes and D.M.P. Souza, Microstructural Development and Microwave Properties of ZnO-Doped Tin Titanate Zirconate, *Mater. Sci. Eng. A*, 2005, **398**, p 220–226
10. G. Wolfran and H.E. Gobel, Existence Range, Structural and Dielectric Properties of $Zr_xTi_ySn_zO4$ ceramics (x + y + z = 2), *Mater. Res. Bull.*, 1981, **16**, p 1455–1463
11. I. Reaney and D.M. Iddles, Microwave Dielectric Ceramics for Resonators and Filters in Mobile Phone Networks, *J. Am. Ceram. Soc.*, 2006, **87**(7), p 2063–2067
12. R. Christoffersen, P.K. Davies, and X. Wei, Effects of Sn Substitution on Cation Ordering in $(Zr_{1-x}Sn0_x)TiO_4$ Microwave Dielectric Ceramics, *J. Am. Ceram. Soc.*, 1994, **77**(6), p 1441–1450
13. Y. Park, Influence of Order-Disorder Transition on Microwave Characteristics of Tin Modified Zirconium Titanate, *J. Mater. Sci. Lett.*, 1995, **14**, p 873–875
14. F. Azough, R. Freer, C.-L. Wang, and G.W. Lorimer, The Relationship Between Microstructure and Microwave Dielectric Properties of Zirconium Titanate Ceramics, *J. Mater. Sci.*, 1996, **31**, p 2539–2549
15. R. Kudesia, A.E. McHale, and R.L. Snyder, Effects of La_2O_3/ZnO Additives on Microstructure And Microwave Dielectric Properties of $Zr_{0.8}Sn_{0.2}TiO_4$ Ceramics, *J. Am. Ceram. Soc.*, 1994, **77**(12), p 3215–3220
16. S. Hirano, T. Hayashi, and A. Hattori, Chemical Processing and Microwave Characteristics of (Zn, Sr)TiO_4 Microwave Dielectrics, *J. Am. Ceram. Soc.*, 1991, **74**(6), p 1320–1324
17. Z.H. Xiong, J.R. Huang, and Z.Y. Pan, Hydrothermal Synthesis of (Zr,Sn)TiO_4 Nano-Powders for Microwave Ceramics, *J. Eur. Ceram. Soc.*, 2003, **23**, p 2515–2518
18. K. Wakino, K. Minai, and H. Tamura, Microwave Characteristics of (Zr,Sn)TiO_4 and BaO-PbO-Nd_2O_3-TiO_2 Dielectric Resonator, *J. Am. Ceram. Soc.*, 1984, **67**(40), p 278–281
19. D.M. Iddles, J. Bell, and A.J. Moulson, Relationships Between Dopants, Microstructure and the Microwave Dielectric Properties of ZrO_2, TiO_2, SnO_2 Ceramics, *J. Mater. Sci.*, 1992, **27**, p 6303–6310
20. Y.H. Park, J.M. Ryu, M.Y. Shin, K.H. Ko, D.W. Kim, and K.-S. Hong, Effect of Nb_2O_5/ZnO Addition on Microwave Properties of $(Zr_{0.8}Sn_{0.2})TiO_4$ Ceramics, *J. Am. Ceram. Soc.*, 2001, **84**(11), p 2542–2546
21. "Standard test methods for determining average grain size," E 112-10, AMERICAN SOCIETY FOR TESTING AND MATERIALS, 2010, 26 p
22. B.W. Hakki and P.D. Colemann, A Dielectric Resonator Method of Measuring Inductive Capacities in the Millimeters Range, *IRE Trans Microwave Theory Tech.*, 1960, **MTT-8**(7), p 402–410